

Multipolar spin liquid in an exactly solvable model for $j_{\text{eff}} = \frac{3}{2}$ moments

Vanuildo S. de Carvalho,¹ Hermann Freire,¹ and Rodrigo G. Pereira²

¹*Instituto de Física, Universidade Federal de Goiás, 74.001-970, Goiânia-GO, Brazil*

²*International Institute of Physics and Departamento de Física Teórica e Experimental, Universidade Federal do Rio Grande do Norte, Campus Universitário, Lagoa Nova, Natal, RN, 59078-970, Brazil*

(Dated: October 17, 2023)

We study an exactly solvable model with bond-directional quadrupolar and octupolar interactions between spin-orbital entangled $j_{\text{eff}} = \frac{3}{2}$ moments on the honeycomb lattice. We show that this model features a multipolar spin liquid phase with gapless fermionic excitations. In the presence of perturbations that break time-reversal and rotation symmetries, we find Abelian and non-Abelian topological phases in which the Chern number evaluates to 0, ± 1 , and ± 2 . We also investigate quantum phase transitions out of the multipolar spin liquid using a parton mean-field approach and orbital wave theory. In the regime of strong integrability-breaking interactions, the multipolar spin liquid gives way to ferroquadrupolar-vortex and antiferro-octupolar ordered phases that harbor a hidden spin- $\frac{1}{2}$ Kitaev spin liquid. Our work unveils mechanisms for unusual multipolar orders and quantum spin liquids in Mott insulators with strong spin-orbit coupling.

I. INTRODUCTION

Quantum spin liquids (QSLs) refer to disordered ground states of interacting spin systems which are characterized by the emergence of fractionalized excitations, topological order, and long-range entanglement [1, 2]. The quest for QSLs stands as one of the most prolific topics of investigation in condensed matter physics, as demonstrated by the growing list of QSL candidates and by notable advances in our theoretical understanding of phases beyond the Landau paradigm [3–5].

A guiding principle in the search for new materials is rooted in the engineering of bond-dependent interactions between $j_{\text{eff}} = \frac{1}{2}$ moments, as found in the exactly solvable model proposed by Kitaev for the honeycomb lattice [6]. This model exhibits a genuine QSL ground state resulting from the fractionalization of $j_{\text{eff}} = \frac{1}{2}$ moments into Majorana fermions and a \mathbb{Z}_2 gauge field. Kitaev interactions appear as the leading term in effective models for spin-orbit-assisted Mott insulators with $4d^5$ and $5d^5$ electronic configuration [7]. Over the last decade, several experiments have indicated the proximity of Kitaev material candidates, such as the iridates $(\text{Na}_{1-x}\text{Li}_x)_2\text{IrO}_3$ [8–10] and $\text{H}_3\text{LiIr}_2\text{O}_6$ [11], to a QSL phase. Special attention has been devoted to the compound $\alpha\text{-RuCl}_3$ [12–14], for which a half-quantized thermal Hall conductance has been reported [13].

In recent years, the search for new systems with QSL ground states has expanded to Mott insulators with effective magnetic moments beyond the $j_{\text{eff}} = \frac{1}{2}$ picture [15, 16]. In that regard, higher-spin Kitaev models were microscopically derived for the honeycomb Mott insulators NiI_2 (d^8 configuration and spin $S = 1$) [17] and CrI_3 (d^3 configuration and $S = \frac{3}{2}$) [18–20].

In contrast to the original spin- $\frac{1}{2}$ Kitaev model, these generalizations are not integrable. Their properties have been studied by semiclassical analysis [21], exact diagonalization [17, 22, 23], the density matrix renormalization group method [24–26], and parton mean-field theory [27].

Remarkably, all these methods point to the existence of a QSL ground state for both $S = 1$ and $S = \frac{3}{2}$. In addition, Mott insulators with $4d^1$ and $5d^1$ configurations have also attracted attention [15, 16]. The effective spin Hamiltonians for these systems are written in terms of $j_{\text{eff}} = \frac{3}{2}$ moments [28] and contain multipolar interactions which can give rise to exotic hidden multipolar orders and even spin-orbital liquid phases [29–37].

In this work, we propose an exactly solvable model for $j_{\text{eff}} = \frac{3}{2}$ moments located on the sites of a honeycomb lattice which could potentially describe some properties of $4d^1$ and $5d^1$ materials. This model involves a combination of nearest-neighbor bond-directional quadrupole-quadrupole and octupole-octupole interactions. The representation of the quadrupolar and octupolar operators in terms of Majorana fermions maps the model to noninteracting fermions hopping on the background of a static \mathbb{Z}_2 gauge field. Since this model exhibits a gapless quantum disordered ground state and spin-orbital correlations associated with the fractionalization of higher magnetic multipoles, it epitomizes all the features of a *multipolar spin liquid* (MSL) [16, 38–40].

Our model should be viewed as an integrable point in the parameter space for the most general model describing $j_{\text{eff}} = \frac{3}{2}$ spin-orbital systems. In this sense, the existence of the MSL offers a different avenue of research in the quest for materials with unusual QSL properties. Indeed, we show that, under the action of rotational and time-reversal-symmetry-breaking fields, our exactly solvable model realizes non-trivial Abelian and non-Abelian topological phases with gapless chiral Majorana modes on the edge. Furthermore, we study the robustness of the MSL state against the formation of long-range multipolar orders driven by integrability-breaking interactions. Interestingly, even in the strong-coupling regime the system exhibits a hidden QSL state described by a spin- $\frac{1}{2}$ Kitaev model on top of either a ferroquadrupolar-vortex (FQV) or an antiferro-octupolar (AO) ordered state.

The remainder of our paper is structured as follows. In Sec. II, we introduce and provide the motivation for the

$j_{\text{eff}} = \frac{3}{2}$ model with bond-directional quadrupolar and octupolar interactions. In Sec. III, we study the properties of the MSL in the exactly solvable limit of the model. While the fully symmetric MSL is gapless, we show that magnetic and strain fields can give rise to Abelian and non-Abelian topological phases. Section IV focuses on the stability of the MSL and the quantum phase transitions out of this state, analyzed using parton mean-field theory and orbital wave theory. Finally, we present our concluding remarks in Sec. V. We leave to Appendixes A and B some technical details on the identification of the lower-energy gauge-flux sector of the MSL and also on the parton mean-field approach employed here.

II. MODEL

We consider interacting local moments with effective total angular momentum $j_{\text{eff}} = \frac{3}{2}$, which appear in Mott insulators with $4d^1$ or $5d^1$ transition-metal ions [16, 28, 41]. The single electron in the open shell occupies the triply degenerate t_{2g} orbitals with effective orbital angular momentum $l_{\text{eff}} = 1$, which in turn are split by the spin-orbit coupling into a higher-energy $j_{\text{eff}} = 1/2$ doublet and a lower-energy $j_{\text{eff}} = 3/2$ quartet. The latter is formed by two Kramers doublets, which may remain degenerate at low temperatures because the strong spin-orbit coupling suppresses the Jahn-Teller effect [42].

An effective spin-orbital Hamiltonian for $j_{\text{eff}} = \frac{3}{2}$ moments was derived in Refs. [32, 33] considering the dominant exchange process on the honeycomb lattice. The starting point is a multiorbital Hubbard-Kanamori model that combines the effects of the crystal electric field, spin-orbit coupling, and electronic correlations, assuming a single hopping path for 90° bonds formed by edge-sharing octahedra. The resulting Hamiltonian contains quadrupole-quadrupole and octupole-octupole interactions with coupling constants of the same order as the coupling between dipole moments. More generally, one should take into account subleading hopping paths known to be important in the generic model for Kitaev materials [43]. Furthermore, the electrostatic interaction between orbitals with different charge distributions and the virtual exchange of optical phonons in the cooperative Jahn-Teller effect can also renormalize the quadrupole-quadrupole interactions [44, 45].

Out of the most general Hamiltonian for $j_{\text{eff}} = \frac{3}{2}$ moments, here we shall focus on the regime of parameter space where the leading interactions involve quadrupole and octupole moments. Such a hierarchy of interactions could in principle be realized in layered materials where the relative strength of the couplings can be tuned by strain [46, 47].

We can label the multipolar operators acting on $j_{\text{eff}} = \frac{3}{2}$ states by irreducible representations of the octahedral group [48]. As shown in Table I, the quadrupole moment has three components, O^γ , with $\gamma \in \{1, 2, 3\} \equiv \{x, y, z\}$, which forms a Γ_5 representation, and two components,

TABLE I. Quadrupolar and octupolar operators acting on $j_{\text{eff}} = \frac{3}{2}$ states. The overlines in $\overline{J^\alpha J^\beta}$ and $\overline{J^\alpha J^\beta J^\gamma}$ stand for a symmetrization with respect to the indices of the dipolar operators J^α , e.g., $\overline{J^x (J^y)^2} \equiv J^x (J^y)^2 + J^y J^x J^y + (J^y)^2 J^x$. Here we omit the octupolar operators that transform in the Γ_4 representation (see, e.g., Ref. [48]).

Moment	Symmetry	Operators
Quadrupole	Γ_3	$O_3 \equiv O^{3z^2-r^2} = \frac{1}{3}[3(J^z)^2 - \mathbf{J}^2]$
		$O_2 \equiv O^{x^2-y^2} = \frac{1}{\sqrt{3}}[(J^x)^2 - (J^y)^2]$
	Γ_5	$O^x \equiv O^{yz} = \frac{1}{\sqrt{3}}\overline{J^y J^z}$
		$O^y \equiv O^{zx} = \frac{1}{\sqrt{3}}\overline{J^x J^z}$
		$O^z \equiv O^{xy} = \frac{1}{\sqrt{3}}\overline{J^x J^y}$
Octupole	Γ_2	$T^{xyz} = \frac{2}{3\sqrt{3}}\overline{J^x J^y J^z}$
	Γ_5	$T^x \equiv T_\beta^x = \frac{2}{3\sqrt{3}}[\overline{J^x (J^y)^2} - \overline{(J^z)^2 J^x}]$
		$T^y \equiv T_\beta^y = \frac{2}{3\sqrt{3}}[\overline{J^y (J^z)^2} - \overline{(J^x)^2 J^y}]$
		$T^z \equiv T_\beta^z = \frac{2}{3\sqrt{3}}[\overline{J^z (J^x)^2} - \overline{(J^y)^2 J^z}]$

O_2 and O_3 , which transform in the Γ_3 representation. From the latter, we define the linear combinations

$$\tilde{O}^\gamma = \cos\left(\frac{2\pi\gamma}{3}\right) O_3 + \sin\left(\frac{2\pi\gamma}{3}\right) O_2, \quad (1)$$

so that a C_3 rotation about the (111) axis perpendicular to the lattice plane acts as $\gamma \mapsto \gamma + 1$ for both O^γ and \tilde{O}^γ . We then consider bond-dependent quadrupole-quadrupole interactions of the form

$$H_q = \sum_{\gamma=x,y,z} \sum_{\langle jl \rangle_\gamma} (K_q O_j^\gamma O_l^\gamma + K'_q \tilde{O}_j^\gamma \tilde{O}_l^\gamma), \quad (2)$$

where $\langle jl \rangle_\gamma$ refers to nearest-neighbor sites along a γ bond of the honeycomb lattice, as in the standard notation for the Kitaev model [5]. The first term in H_q can be generated by integrating out vibronic couplings to trigonal distortions, which are significant in some cubic d^1 systems [41, 49]. This term was considered in the model for a quadrupolar spin liquid defined in Ref. [35]. The model with the pure K_q interaction has a macroscopically degenerate ground-state manifold [35]. Adding perturbations to this special point in the phase diagram, we can access different phases with exotic multipolar orders or spin-orbital liquid behavior. On the other hand, the second term in Eq. (2) can be generated by coupling to tetragonal distortions or by electrostatic interactions [28]. This term is known to favor quadrupolar order with a vortex pattern [50, 51].

We now add octupole-octupole interactions to our model. To reduce the number of parameters, we focus on interactions that involve the components transforming in the Γ_2 and Γ_5 representations shown in Table I. This means that we neglect the octupolar operators, which, like the dipole moment \mathbf{J} , transform in the Γ_4 representation [48]. As we shall see in Sec. III, this choice is convenient for the purpose of identifying exactly solvable limits of the general model. We then consider

$$H_o = \sum_{\gamma=x,y,z} \sum_{\langle jl \rangle_\gamma} (K_o T_j^\gamma T_l^\gamma + K'_o T_j^{xyz} T_l^{xyz}). \quad (3)$$

Note that the octupolar operators are odd under time reversal, but the interactions are time-reversal invariant. A bond-dependent octupolar interaction similar to the first term in Eq. (3) appears in phenomenological models for the hidden multipolar order in the heavy-fermion compound $\text{Ce}_x\text{La}_{1-x}\text{B}_6$ [52, 53]. The second term in Eq. (3) favors an octupolar order without lattice distortions analogous to the one proposed for double perovskites with $j_{\text{eff}} = 2$ local moments [54, 55]. Altogether, the Hamiltonian $H = H_q + H_o$ captures the competition between different types of multipolar order.

To analyze the multipolar interactions, it is useful to express the $j_{\text{eff}} = \frac{3}{2}$ states in terms of pseudospin and a pseudo-orbital degrees of freedom [29, 30, 35, 56]. The local Hilbert space is spanned by the eigenstates $|m_J\rangle$ of J^z , which obey $J^z|m_J\rangle = m_J|m_J\rangle$, with $m_J \in \{\pm\frac{1}{2}, \pm\frac{3}{2}\}$. We define the mapping

$$|m_J = \frac{3}{2}\rangle = |s^z = -\frac{1}{2}, \tau^z = \frac{1}{2}\rangle, \quad (4)$$

$$|m_J = \frac{1}{2}\rangle = -|s^z = \frac{1}{2}, \tau^z = -\frac{1}{2}\rangle, \quad (5)$$

$$|m_J = -\frac{1}{2}\rangle = |s^z = -\frac{1}{2}, \tau^z = -\frac{1}{2}\rangle, \quad (6)$$

$$|m_J = -\frac{3}{2}\rangle = -|s^z = \frac{1}{2}, \tau^z = \frac{1}{2}\rangle, \quad (7)$$

where \mathbf{s}_j and $\boldsymbol{\tau}_j$ are, respectively, pseudospin and pseudo-orbital operators, which obey the SU(2) algebra $[s_j^\alpha, s_j^\beta] = i\epsilon^{\alpha\beta\gamma}\delta_{jk}s_j^\gamma$ and $[\tau_j^\alpha, \tau_j^\beta] = i\epsilon^{\alpha\beta\gamma}\delta_{jk}\tau_j^\gamma$ and the relation $[s_j^\alpha, \tau_j^\beta] = 0$. In the $\{|s^z, \tau^z\rangle\}$ basis, the quadrupolar and octupolar operators given in Table I become

$$\begin{aligned} O^\gamma &= -4s^\gamma\tau^y, & O_3 &= 2\tau^z, & O_2 &= 2\tau^x, \\ T^\gamma &= -4s^\gamma\mathbf{v}^\gamma \cdot \boldsymbol{\tau}, & T^{xyz} &= 2\tau^y, \end{aligned} \quad (8)$$

where $\mathbf{v}^\gamma = \cos(2\pi\gamma/3)\hat{\mathbf{x}} - \sin(2\pi\gamma/3)\hat{\mathbf{z}}$ are unit vectors in the xz plane of pseudo-orbital space.

III. EXACTLY SOLVABLE MODEL

In this section, we analyze the Hamiltonian $H = H_q + H_o$ in the special limit $K'_q = K'_o = 0$, in which we obtain

$$H_s = \sum_{\gamma=x,y,z} \sum_{\langle jl \rangle_\gamma} (K_q O_j^\gamma O_l^\gamma + K_o T_j^\gamma T_l^\gamma). \quad (9)$$

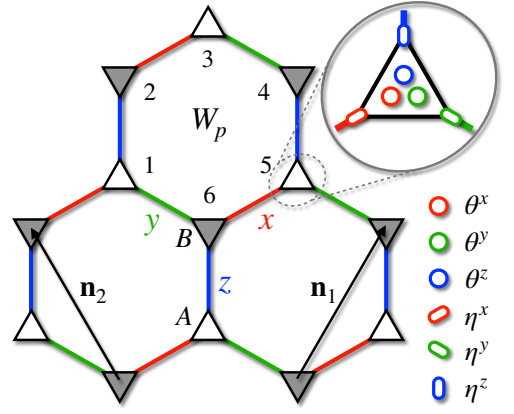


FIG. 1. Schematic representation of fractionalized $j_{\text{eff}} = \frac{3}{2}$ moments on the honeycomb lattice. Here x , y , and z bonds are represented by red, green, and blue solid lines, respectively. The two sublattices, A and B, are represented by up-pointing and down-pointing triangles. The inset in the top right corner shows the matter (θ^γ) and gauge (η^γ) Majorana fermions. Each plaquette is associated with the conserved quantity $\hat{W}_p = -e^{i\pi(J_1^x + J_2^y + J_3^z + J_4^x + J_5^y + J_6^z)}$.

We show that this model can be solved exactly using a Majorana fermion representation for the multipolar operators and exhibits a MSL ground state.

We can write the pseudospin and pseudo-orbital operators in terms of six Majorana fermions as [29, 35]

$$s_j^\gamma = -\frac{i}{4}\epsilon^{\alpha\beta\gamma}\eta_j^\alpha\eta_j^\beta, \quad (10)$$

$$\tau_j^\gamma = -\frac{i}{4}\epsilon^{\alpha\beta\gamma}\theta_j^\alpha\theta_j^\beta, \quad (11)$$

where $\epsilon^{\alpha\beta\gamma}$ is the Levi-Civita tensor and η^α and θ^α are Majorana fermion operators which obey the algebra $\{\eta_j^\alpha, \eta_k^\beta\} = 2\delta_{jk}\delta^{\alpha\beta}$, $\{\theta_j^\alpha, \theta_k^\beta\} = 2\delta_{jk}\delta^{\alpha\beta}$, and $\{\eta_j^\alpha, \theta_k^\beta\} = 0$. This Majorana representation enlarges the Hilbert space, introducing unphysical states. To avoid that, we impose the local constraint

$$D_j \equiv i\eta_j^x\eta_j^y\eta_j^z\theta_j^x\theta_j^y\theta_j^z = 1 \quad (12)$$

for every site j . This is equivalent to obtaining a physical state $|\Psi\rangle_{\text{phys}}$ from the Majorana wave function $|\Psi_0\rangle$ by implementing the projection $|\Psi\rangle_{\text{phys}} = \Pi_j[\frac{1}{2}(1 + D_j)]|\Psi_0\rangle$. Using the local constraint and the expressions in Eq. (8), we can write the multipolar operators as Majorana bilinears:

$$\begin{aligned} O^\gamma &= i\eta^\gamma\theta^y, & O_3 &= -i\theta^x\theta^y, & O_2 &= -i\theta^y\theta^z, \\ T^\gamma &= -i\eta^\gamma(\mathbf{v}^\gamma \cdot \boldsymbol{\theta}), & T^{xyz} &= -i\theta^z\theta^x. \end{aligned} \quad (13)$$

Note that $\mathbf{v}^\gamma \cdot \boldsymbol{\theta} = \cos(2\pi\gamma/3)\theta^x - \sin(2\pi\gamma/3)\theta^z$ only involves only θ^x and θ^z .

Using the Majorana representation, we cast the Hamiltonian in the form

$$H_s = i \sum_{\gamma} \sum_{\langle jl \rangle_\gamma} \hat{u}_{\langle jl \rangle_\gamma} [K_q \theta_j^y \theta_l^y + K_o (\mathbf{v}^\gamma \cdot \boldsymbol{\theta}_j) (\mathbf{v}^\gamma \cdot \boldsymbol{\theta}_l)], \quad (14)$$

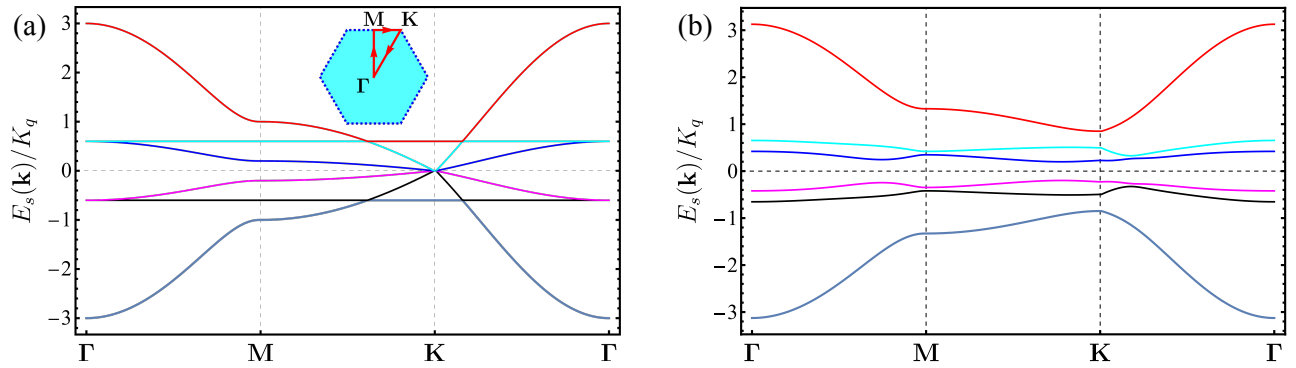


FIG. 2. Dispersion relation for Majorana fermion excitations in the exactly solvable MSL model. Here we set $K_o = 0.4K_q$. (a) For the unperturbed model in Eq. (9), the system exhibits a gapless spectrum with Dirac nodes at the \mathbf{K} point. (b) In the presence of strain fields ε_2 and ε_3 and time-reversal-symmetry-breaking field h [see Eq. (17)], the excitation spectrum becomes gapped. Here we set $\varepsilon_2 = \varepsilon_3 = 0.4K_q$ and $h = 0.1K_q$.

where $\hat{u}_{\langle jl \rangle \gamma} \equiv -in_j^\gamma \eta_l^\gamma$ are antisymmetric bond operators obeying $\hat{u}_{\langle jl \rangle \gamma} = -\hat{u}_{\langle lj \rangle \gamma}$. These operators commute with each other and define \mathbb{Z}_2 gauge fields since H_s is invariant with respect to the local transformations $\theta_j^\gamma \mapsto \Lambda_j \theta_j^\gamma$ and $\hat{u}_{\langle jl \rangle \gamma} \mapsto \Lambda_j \hat{u}_{\langle jl \rangle \gamma} \Lambda_l$, with $\Lambda_j = \pm 1$. Like what happens for the dipolar Kitaev models [6, 21], the Hamiltonian in Eq. (9) possesses a conserved operator $\hat{W}_p \equiv -e^{i\pi(J_1^x + J_2^y + J_3^z + J_4^x + J_5^y + J_6^z)}$ for each hexagonal plaquette p . In the Majorana representation, the plaquette operators read $\hat{W}_p = \prod_{\langle j,l \rangle \gamma \in p} \hat{u}_{\langle j,l \rangle \gamma}$ [27, 35]. Due to the form of the Hamiltonian in Eq. (14), we refer to η^γ as the gauge fermions and to θ^γ as the matter fermions. The fractionalization of the multipolar operators into Majorana fermions is illustrated in Fig. 1.

We verified numerically that the ground state of H_s lies in the sector where the eigenvalues of all conserved plaquette operators are set to $W_p = +1$ (see Appendix A). Fixing a gauge configuration with $u_{\langle jl \rangle \gamma} = 1$ for sites j in sublattice A and l in sublattice B, we obtain from

$$E_s(\mathbf{k}) = \pm \frac{|K_o|}{\sqrt{2}} \sqrt{|g_z(\mathbf{k})|^2 + |g_x(\mathbf{k})|^2 + 2|g_{xz}(\mathbf{k})|^2} \pm \sqrt{[|g_z(\mathbf{k})|^2 - |g_x(\mathbf{k})|^2]^2 + 4|g_x(\mathbf{k})g_{xz}^*(\mathbf{k}) + g_z^*(\mathbf{k})g_{xz}(\mathbf{k})|^2}, \quad (16)$$

where we define the functions $g_z(\mathbf{k}) = \frac{3}{4}(e^{i\mathbf{k}\cdot\mathbf{n}_1} + e^{i\mathbf{k}\cdot\mathbf{n}_2})$, $g_x(\mathbf{k}) = 1 + \frac{1}{4}(e^{i\mathbf{k}\cdot\mathbf{n}_1} + e^{i\mathbf{k}\cdot\mathbf{n}_2})$, and $g_{xz}(\mathbf{k}) = \frac{\sqrt{3}}{4}(e^{i\mathbf{k}\cdot\mathbf{n}_1} - e^{i\mathbf{k}\cdot\mathbf{n}_2})$.

The band structure of the Majorana fermion excitations is shown in Fig. 2(a). The spectrum exhibits gapless modes with Dirac cones at the \mathbf{K} point in both sectors associated with θ^y fermions and mixed θ^x and θ^z fermions. The latter sector also displays a completely flat gapped band. This peculiar feature holds for only the model with spatially isotropic couplings; the gapped band becomes dispersive as soon as we introduce different octupolar couplings $K_o^{(\gamma)}$ for each bond direction γ .

Eq. (14) a translation-invariant quadratic Hamiltonian for the matter fermions moving in the background of the static \mathbb{Z}_2 gauge field. Note that the θ^y fermion decouples from θ^x and θ^z . The dynamics of θ^y is governed by the quadrupolar coupling K_q , whereas the dynamics of θ^x and θ^z depends on the octupolar coupling K_o . We diagonalize the Hamiltonian using the Fourier transform

$$\theta_b^\gamma(\mathbf{R}) = \sqrt{\frac{2}{N}} \sum_{\mathbf{k} \in \frac{1}{2}(\text{BZ})} [e^{-i\mathbf{k}\cdot\mathbf{R}} \theta_b^\gamma(\mathbf{k}) + e^{i\mathbf{k}\cdot\mathbf{R}} \theta_b^{\gamma\dagger}(\mathbf{k})], \quad (15)$$

where \mathbf{R} is the position of the unit cell, $b \in \{A, B\}$ refers to the sublattice index, N is the number of sites, and the momentum sum runs over half of the Brillouin zone (BZ). The bands associated with the θ^y fermions have the dispersion relation $E_s(\mathbf{k}) = \pm |K_q g_y(\mathbf{k})|$, where $g_y(\mathbf{k}) = 1 + e^{i\mathbf{k}\cdot\mathbf{n}_1} + e^{i\mathbf{k}\cdot\mathbf{n}_2}$, with lattice vectors $\mathbf{n}_1 = \frac{\sqrt{3}}{2}(1, \sqrt{3})$ and $\mathbf{n}_2 = \frac{\sqrt{3}}{2}(-1, \sqrt{3})$. For the bands associated with θ^x and θ^z , we obtain

Importantly, by generating a dispersion for θ^x and θ^z fermions, the octupolar interaction lifts the macroscopic degeneracy of the pure quadrupolar model [35]. Consequently, our exactly solvable model stabilizes a unique MSL ground state.

In addition to gapless Majorana fermions, the spectrum of H_s contains vortex excitations (visons) associated with changing the eigenvalues of the plaquette operators to $W_p = -1$. These gapped excitations are created in pairs by the action of local operators which anticommute with the bond operators $\hat{u}_{\langle jl \rangle \gamma}$. Remarkably, the quadrupole operators O_2 and O_3 and the octupolar op-

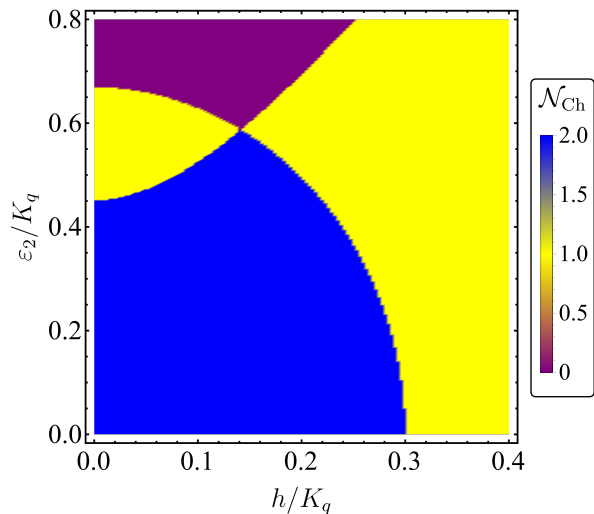


FIG. 3. Topological phase diagram of the MSL as a function of the symmetry-breaking fields ε_2 and h . Here we set $K_o = 0.2K_q$ and $\varepsilon_2 = \varepsilon_3$. The purple, yellow, and blue regions correspond to Chern numbers 0, 1, and 2, respectively.

erator T^{xyz} do not excite visons since they commute with the gauge fermions [see Eq. (13)]. As a result, O_2 , O_3 , and T^{xyz} are the only on-site operators featuring a gapless spectrum in the corresponding dynamical structure factors probed by resonant inelastic x-ray scattering [30]. By contrast, the dynamical spin structure factor for the pure Kitaev model exhibits a flux gap [57].

In analogy with the Kitaev model, we can drive the MSL to topological phases by adding perturbations that break symmetries and gap out the fermionic spectrum. We can break the \mathbb{Z}_3 symmetry (rotation in real and spin-orbital space) and time-reversal symmetry while still preserving the integrability of the model if we consider the perturbations

$$\delta H_s = - \sum_j (\varepsilon_2 O_{2,j} + \varepsilon_3 O_{3,j} + h T_j^{xyz}). \quad (17)$$

Here ε_2 and ε_3 describe tetragonal strain fields and h induces an octupole moment, allowed by symmetry in the presence of an external magnetic field. According to Eq. (13), the total Hamiltonian remains quadratic in the matter fermions, but the strain fields couple θ^y to θ^x and θ^z . As shown in Fig. 2(b), we find a fully gapped spectrum for generic values of ε_2 , ε_3 , and h . However, there exist critical values of these parameters for which the Majorana gap closes and then reopens, which is suggestive of topological phase transitions.

To investigate the topological nature of the gapped phases, we evaluate the Chern number

$$\mathcal{N}_{\text{Ch}} \equiv \frac{1}{2\pi} \sum_n \int_{\text{BZ}} d^2\mathbf{k} \mathcal{B}_n(\mathbf{k}), \quad (18)$$

where $\mathcal{B}_n(\mathbf{k}) = [\nabla \times \mathcal{A}_n(\mathbf{k})]_z$ is the Berry curvature associated with the n th energy band; $\mathcal{A}_n(\mathbf{k}) =$

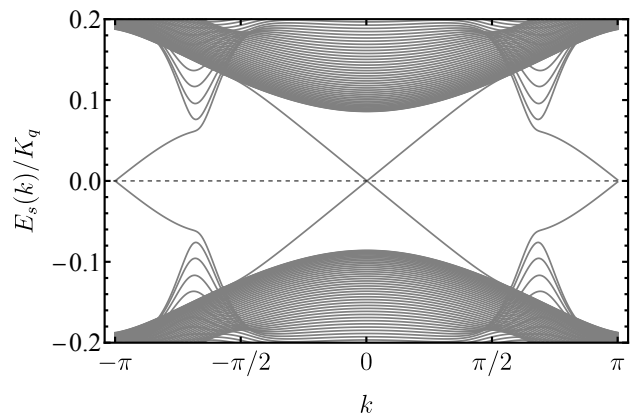


FIG. 4. Edge states of the MSL for a honeycomb lattice with zigzag edges. Here we use a cylinder with $L = 50$ unit cells along the open direction. We fix the parameters as $K_o = h = \varepsilon_2 = \varepsilon_3 = 0.2K_q$ in the regime of $\mathcal{N}_{\text{Ch}} = \pm 2$ (see Fig. 3).

$i\langle u_n(\mathbf{k}) | \nabla_{\mathbf{k}} | u_n(\mathbf{k}) \rangle$ is the Berry connection, with $|u_n(\mathbf{k})\rangle$ being the eigenvectors of the Hamiltonian; and the sum on the right-hand-side runs over the occupied bands. We determine \mathcal{N}_{Ch} numerically following the approach devised in Ref. [58]. The dependence of \mathcal{N}_{Ch} on the symmetry-breaking fields is shown in Fig. 3. Remarkably, the interplay between strain and magnetic fields realizes five of Kitaev's 16-fold-way phases [6, 59, 60]: a trivial phase with $\mathcal{N}_{\text{Ch}} = 0$, two non-Abelian topological phases with $\mathcal{N}_{\text{Ch}} = \pm 1$, and two Abelian topological phases with $\mathcal{N}_{\text{Ch}} = \pm 2$. For $0 < |\varepsilon_2|, |\varepsilon_3|$ and $|h| \ll |K_q|$, the system is in an Abelian phase with $\mathcal{N}_{\text{Ch}} = \pm 2$, depending on the sign of h . We can reach the non-Abelian phase by increasing the strength of the symmetry-breaking fields, whereas the trivial phase appears only for strong strain fields. Varying the ratio K_o/K_q , we observe that enhancing the octupolar interaction favors the Abelian phase. We have verified that the Majorana gap closes at topological phase transitions where the Chern number changes. The momentum at which the gap closes depends on the interactions and is not attached to the \mathbf{K} point. A direct transition from $\mathcal{N}_{\text{Ch}} = \pm 2$ to $\mathcal{N}_{\text{Ch}} = 0$ is possible by fine tuning so that the gap closes simultaneously at two different points in the Brillouin zone.

As a signature of the topological phases, we look for chiral edge states in a cylinder geometry with zigzag edges. The result matches the Chern number, in accordance with the bulk-boundary correspondence. Figure 4 shows the spectrum with two chiral edge states in the regime where $\mathcal{N}_{\text{Ch}} = \pm 2$. The chiral edge states can be probed by the thermal Hall conductance κ_{xy} , which for low enough temperatures behaves as $\kappa_{xy} = \frac{\mathcal{N}_{\text{Ch}}}{2} \frac{\pi k_B^2}{6\hbar} T$.

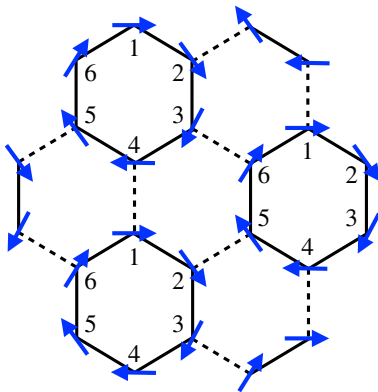


FIG. 5. Schematic representation of the ferroquadrupolar-vortex state on the honeycomb lattice. The arrows represent the direction of the vector defined by $(\langle O_2 \rangle, \langle O_3 \rangle) = 2(\langle \tau^x \rangle, \langle \tau^z \rangle) \propto (\cos \phi_n, -\sin \phi_n)$, where $\phi_n = (n-1)\pi/3$, with $n = 1, \dots, 6$ being the sublattice index.

IV. MULTIPOLAR ORDERS FROM INTEGRABILITY-BREAKING INTERACTIONS

In this section, we address the effect of the interactions K'_q and K'_o in Eqs. (2) and (3) on the ground state and elementary excitations of the spin-orbital system. We define

$$H_I = \sum_{\gamma} \sum_{\langle j \rangle_{\gamma}} (K'_q \tilde{O}_j^{\gamma} \tilde{O}_l^{\gamma} + K'_o T_j^{xyz} T_l^{xyz}), \quad (19)$$

so that $H = H_q + H_o = H_s + H_I$. Hereafter we assume that all coupling constants are positive. In the Majorana representation in Eq. (13), H_I gives rise to interaction terms which spoil the integrability of the model. For this reason, we resort to two complementary analytical approximations which provide a qualitative picture of the excitation spectrum, namely parton mean-field theory and orbital wave theory.

A. Parton mean-field theory

For small K'_q and K'_o , we can start from the solution in Sec. III to investigate quantum phase transitions out of the MSL state. We first notice that the quartic terms contained in H_I involve only the matter fermions θ^{γ} . Thus, at least at weak coupling they do not alter the gauge-flux configuration in the ground state, and we can work in the sector with fixed $W_p = 1$ for all plaquettes.

Next, we treat the interactions within a parton mean-field approach [3, 27]. To search for multipolar orders, we use the mean-field decoupling

$$\tilde{O}_j^{\gamma} \tilde{O}_l^{\gamma} \mapsto \langle \tilde{O}_j^{\gamma} \rangle \tilde{O}_l^{\gamma} + \langle \tilde{O}_l^{\gamma} \rangle \tilde{O}_j^{\gamma} - \langle \tilde{O}_j^{\gamma} \rangle \langle \tilde{O}_l^{\gamma} \rangle, \quad (20)$$

$$\begin{aligned} T_j^{xyz} T_l^{xyz} &\mapsto \langle T_j^{xyz} \rangle T_l^{xyz} + T_j^{xyz} \langle T_l^{xyz} \rangle \\ &\quad - \langle T_j^{xyz} \rangle \langle T_l^{xyz} \rangle. \end{aligned} \quad (21)$$

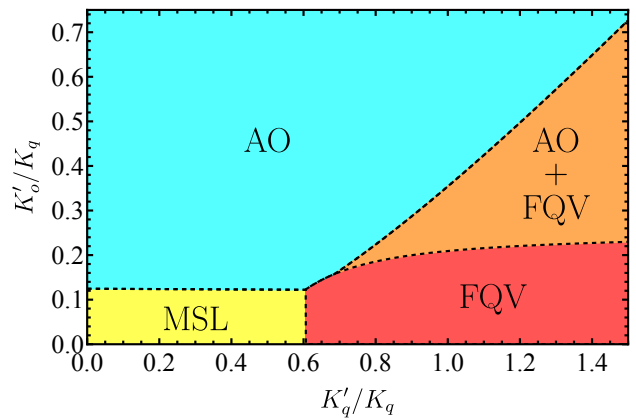


FIG. 6. Ground-state phase diagram obtained from the parton mean-field theory setting $K_o = 0.2K_q$. Here AO and FQV refer to the antiferro-octupolar and ferroquadrupolar-vortex phases, respectively. In addition, the system exhibits a phase with coexisting AO and FQV orders.

The quadrupolar interaction K'_q is equivalent to an orbital compass model on the honeycomb lattice [50, 51] and favors a six-sublattice FQV state that breaks rotational and translational symmetries (see Fig. 5). We parametrize the quadrupolar order parameter as

$$\langle \tilde{O}_j^{\gamma} \rangle = \rho \sum_{\mu=1}^2 f_{\mu}^{\gamma}(\varphi) \cos(\mathbf{Q}_{\mu} \cdot \mathbf{R}_j). \quad (22)$$

Here ρ and φ are variational parameters, the functions $f_{\mu}^{\gamma}(\varphi)$ are given by $f_1^{\gamma}(\varphi) = \sin(2\pi\gamma/3 - \varphi)$ and $f_2^{\gamma}(\varphi) = \cos(2\pi\gamma/3 - \varphi)$, and the wave vectors $\mathbf{Q}_1 = \frac{\pi}{\sqrt{3}}(\sqrt{3}, 1)$ and $\mathbf{Q}_2 = \frac{\pi}{\sqrt{3}}(-\sqrt{3}, 1)$ connect high-symmetry points of the reciprocal lattice [61]. On the other hand, for $K'_o > 0$ the octupolar order parameter $\langle T_j^{xyz} \rangle$ is constrained to having the familiar form for antiferromagnetic order on a bipartite lattice, i.e.,

$$\langle T_j^{xyz} \rangle = \begin{cases} +\chi & \text{if } j \in A, \\ -\chi & \text{if } j \in B. \end{cases} \quad (23)$$

A nonzero value of χ implies a phase with AO order.

The precise form of the mean-field Hamiltonian can be found in Appendix B. From this Hamiltonian, we obtain the free energy

$$\begin{aligned} \mathcal{F}_{\text{MF}} &= -T \sum_{\ell=1}^{18} \int_{\frac{1}{6}(\text{BZ})} \frac{d^2\mathbf{k}}{\mathcal{A}_{\text{BZ}}} \ln [1 + e^{-\beta E_{\ell}(\mathbf{k})}] \\ &\quad + K'_q [\mathcal{A}_0 - \mathcal{B}_0 \sin(2\varphi)] \rho^2 + 3K'_o \chi^2, \end{aligned} \quad (24)$$

where $\beta = 1/T$ is the inverse temperature and

$$\mathcal{A}_0 \equiv \left| 2 \cos\left(\frac{\pi}{\sqrt{3}}\right) + \cos\left(\frac{2\pi}{\sqrt{3}}\right) \right| \approx 1.365, \quad (25)$$

$$\mathcal{B}_0 \equiv \sqrt{3} \sin\left(\frac{\pi}{2\sqrt{3}}\right) \sin\left(\frac{\sqrt{3}\pi}{2}\right) \approx 0.557. \quad (26)$$

In addition, $\mathcal{A}_{\text{BZ}} = 8\pi^2/(3\sqrt{3})$ refers to the area of the BZ and $E_\ell(\mathbf{k})$ are the dispersion relations obtained by numerical diagonalization of the mean-field Hamiltonian.

To determine the mean-field parameters ρ , φ , and χ , we numerically minimize the free energy in the zero-temperature limit by means of a random-search algorithm which finds the lowest value of \mathcal{F}_{MF} from a set of randomly chosen initial conditions. The ground-state phase diagram as a function of the integrability-breaking perturbations for fixed $K_o = 0.2K_q$ is shown in Fig. 6. First, we note that the MSL phase is stable as long as K_q and K_o are both nonzero and there are no zero-energy flat bands in the spectrum of the unperturbed model. As we increase K'_o , the MSL undergoes a quantum phase transition to a state with AO order, $\chi \neq 0$, which spontaneously breaks time-reversal symmetry. On the other hand, if we start from the solvable model and increase K'_q , the system develops FQV order with $\rho \neq 0$, breaking lattice rotation and translation symmetries. In this regime, we find that the parameter φ evaluates to either $\varphi = \pi/4$ or $\varphi = 5\pi/4$. This degeneracy is associated with the invariance of the Hamiltonian under inversion of all quadrupole moments, which follows from $f_\mu^\gamma(\varphi + \pi) = -f_\mu^\gamma(\varphi)$. Finally, when K'_q and K'_o are comparable, the phase diagram exhibits a coexistence region between the FQV and AO phases. Within our mean-field approach, all phase transitions are of first order.

We now analyze the dispersion relation of the Majorana fermions in the ordered phases. Representative results for the AO, FQV, and coexistence phases are shown in Fig. 7. In the AO phase, the mean-field decoupling with $\chi \neq 0$ introduces a staggered on-site term that couples θ^x and θ^z without affecting θ^y . As a result, the spectrum remains gapless with a Dirac node at the \mathbf{K} point [see Fig. 7(a)]. By contrast, in the FQV phase the mean-field Hamiltonian with $\rho \neq 0$ couples all three flavors of Majorana fermions. In this case, we obtain a fully gapped spectrum [see Fig. 7(b)]. In the coexistence region, we find that the gap closes as one of the bands crosses zero energy, forming a Majorana Fermi surface [see Fig. 7(c)]. Note that the spectrum is not particle-hole symmetric because the on-site terms break the chiral symmetry in the mean-field Hamiltonian.

B. Orbital wave theory

In the regime $K'_q, K'_o \gg K_q, K_o$, the mean-field approximation used in the previous section is no longer reliable because the strong integrability-breaking interactions are able to create vison excitations. However, we can go the other way and consider the MSL Hamiltonian H_s to be a small perturbation to H_I . It is instructive to rewrite the Hamiltonian in terms of the pseudospin and

pseudo-orbital operators using Eq. (8):

$$\begin{aligned} H_I &= 4K'_q \sum_\gamma \sum_{\langle jl \rangle_\gamma} (\mathbf{u}^\gamma \cdot \boldsymbol{\tau}_j)(\mathbf{u}^\gamma \cdot \boldsymbol{\tau}_l) + 4K'_o \sum_{\langle jl \rangle} \tau_j^y \tau_l^y, \\ H_s &= 16K_q \sum_\gamma \sum_{\langle jl \rangle_\gamma} (s_j^\gamma \tau_j^y)(s_l^\gamma \tau_l^y) \\ &\quad + 16K_o \sum_\gamma \sum_{\langle jl \rangle_\gamma} (s_j^\gamma \mathbf{v}^\gamma \cdot \boldsymbol{\tau}_j)(s_l^\gamma \mathbf{v}^\gamma \cdot \boldsymbol{\tau}_l), \end{aligned} \quad (27)$$

where $\mathbf{u}^\gamma = \mathbf{v}^\gamma \times \hat{\mathbf{y}} = \sin(2\pi\gamma/3)\hat{\mathbf{x}} + \cos(2\pi\gamma/3)\hat{\mathbf{z}}$. Clearly, H_I describes interactions within the pseudo-orbital sector. For $K'_q, K'_o \gg K_q, K_o$, we expect $\boldsymbol{\tau}_j$ to develop long-range order first, and the resulting ordered state determines the effective interactions in the pseudospin sector at a lower energy scale.

Let us consider the classical ground states of H_I , with pseudo-orbitals treated as vectors with length τ . The FQV phase corresponds to a vortex state with $\boldsymbol{\tau}$ vectors in the xz plane, as illustrated in Fig. 5. In the AO phase, the $\boldsymbol{\tau}$ vectors point along the y axis. If we consider a state that interpolates between FQV and AO configurations, with orbital vectors forming an angle θ with the $\pm\hat{\mathbf{y}}$ direction (alternating between A and B sublattices), the corresponding energy per site is

$$E_{\text{cl}}(\theta) = -3\tau^2(K'_q \sin^2 \theta + 2K'_o \cos^2 \theta). \quad (28)$$

Minimizing this energy, we obtain a direct transition between AO order ($\theta = 0$) and FQV order ($\theta = \pi/2$) at $K'_o = K'_q/2$. In contrast to the mean-field theory in Sec. IV A, this classical analysis in the strong-coupling limit does not support the presence of a coexistence region in the phase diagram.

We can go beyond the classical analysis and compute quantum corrections using linear orbital wave theory [50, 62, 63]. The first step is to rotate the pseudo-orbital operators to the local polarization axis in either FQV or AO states. We write $\boldsymbol{\tau}_j = R_j^T \tilde{\boldsymbol{\tau}}_j$, where R_j is a 3×3 orthogonal matrix that implements the appropriate position-dependent rotation. In the rotated frame, we employ the Holstein-Primakoff transformation

$$\tilde{\tau}_j^z = \tau - a_j^\dagger a_j, \quad (29)$$

$$\tilde{\tau}_j^\pm = a_j^\dagger (2\tau - a_j^\dagger a_j)^{1/2}, \quad (30)$$

where a_j^\dagger and a_j are bosonic creation and annihilation operators. The effective Hamiltonian to order τ is quadratic in the bosonic operators and can be diagonalized by a Bogoliubov transformation. We then obtain

$$H_I \approx \sum_{\nu, \mathbf{k}} \omega_\nu(\mathbf{k}) \alpha_\nu^\dagger(\mathbf{k}) \alpha_\nu(\mathbf{k}) + E_0, \quad (31)$$

where $\omega_\nu(\mathbf{k})$ is the dispersion relation of the quantized pseudo-orbital waves in the FQV or AO states, with ν being the band index and $\alpha_\nu(\mathbf{k})$ being the corresponding boson annihilation operator, and

$$E_0 = -3N\tau(\tau + 1)\mathcal{E} + \frac{1}{2} \sum_{\nu, \mathbf{k}} \omega_\nu(\mathbf{k}) \quad (32)$$

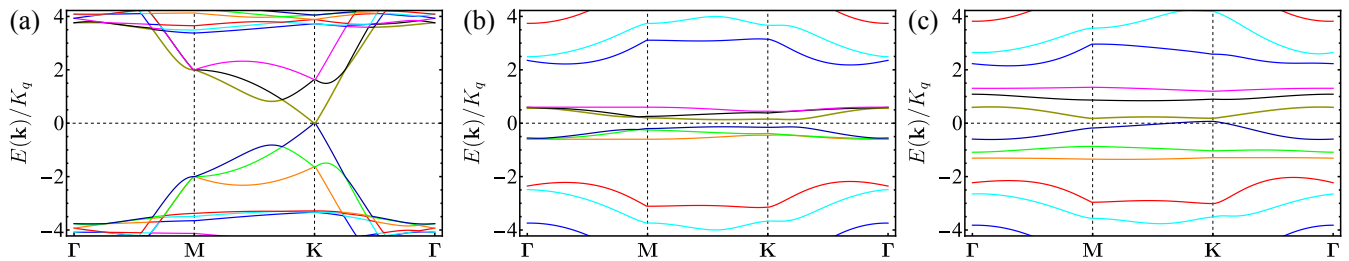


FIG. 7. Energy dispersion of the mean-field Hamiltonian for $K_o = 0.2K_q$, $K'_q = 1.3K_q$, and three different values of K'_o in the broken-symmetry phases: (a) $K'_o = 0.65K_q$ in the AO phase, (b) $K'_o = 0.10K_q$ in the FQV phase, and (c) $K'_o = 0.40K_q$ in the coexistence region. Here the Brillouin zone is defined with respect to the unit cell shown in Fig. 1.

is the ground state energy including the quantum correction, with $\mathcal{E} = K'_o$ in the FQV state and $\mathcal{E} = 2K'_o$ in the AO state.

Perturbative stability of the ordered states against quantum fluctuations requires $\omega_\nu(\mathbf{k})$ to be real and positive for all bands. Using this criterion, we find that the FQV state remains locally stable for $K'_o < 0.746K'_q$, beyond the point $K'_o = K'_q/2$ where its classical energy becomes higher than that of the AO state. Consistently, the quantum correction to the ground-state energy of the AO state is real for $K'_o > K'_q/2$ (see Fig. 8). In the AO phase, the pseudo-orbital wave spectrum is gapped, as expected since the ground state breaks only discrete symmetries. In the FQV phase, the spectrum contains a zero-energy flat band. As emphasized in Ref. [50], the classical FQV state has an $SO(2)$ degeneracy which is lifted by quantum fluctuations, and the quantum corrections select states that maximize the number of zero-energy modes. The gap in the low-energy band in the FQV phase appears only beyond the linear orbital wave theory [51]. Since the excitation spectrum indicates a perturbative stability of the ordered states in the corresponding regimes, with an energy level crossing around $K'_o = K'_q/2$, we conclude that the orbital wave theory points to a first-order transition between FQV and AO phases.

We can now derive an effective Hamiltonian for the pseudospins using a mean-field decoupling of H_s in which the pseudo-orbital degrees of freedom are frozen in the ground state of H_I . This is a standard approach to analyze the low-energy excitations of spin-orbital models [64]. We obtain from Eq. (27)

$$H_s^{\text{eff}} = \sum_{\gamma=x,y,z} \sum_{\langle jl \rangle_\gamma} \mathcal{K}_{jl}^\gamma s_j^\gamma s_l^\gamma, \quad (33)$$

where

$$\mathcal{K}_{jl}^\gamma = -16K_o \langle \tau_j^y \tau_l^y \rangle - 16K_q \langle (\mathbf{v}^\gamma \cdot \boldsymbol{\tau}_j)(\mathbf{v}^\gamma \cdot \boldsymbol{\tau}_l) \rangle. \quad (34)$$

The effective Hamiltonian in Eq. (33) has the precise form of a Kitaev model for pseudospin- $\frac{1}{2}$ moments. As a consequence, the fate of the system in the regime $K'_q, K'_o \gg K_q, K_o$ is to exhibit a *hidden* Kitaev spin liquid on top of classical AO or FQV phases. This feature

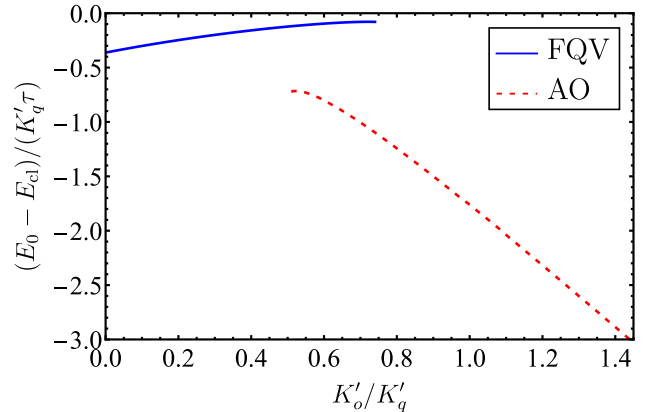


FIG. 8. Quantum correction to the ground-state energy of FQV and AO states [see Eqs. (28) and (32)]. The dispersion relation of pseudo-orbital waves in the FQV state becomes complex for $K'_o > 0.746K'_q$, signaling an instability. Similarly, the AO state becomes unstable for $K'_o < 0.5K'_q$.

bears some resemblance to the behavior of the spin- $\frac{3}{2}$ Kitaev model studied in Ref. [27], in which a spin- $\frac{1}{2}$ Kitaev model emerges in the presence of a single-ion anisotropy that induces a uniform spin quadrupole moment. In our case, the Kitaev spin liquid arises either from octupolar order for $K'_o \gg K'_q$ or from translation-symmetry-breaking quadrupolar order for $K'_q \gg K'_o$.

The pseudospin excitation spectrum depends on the effective Kitaev couplings in Eq. (34). We determine these couplings by computing the pseudo-orbital correlations within the linear orbital wave theory. In the AO phase, which preserves the \mathbb{Z}_3 symmetry, we obtain homogeneous antiferromagnetic coupling $\mathcal{K}_{jl}^\gamma = \mathcal{K} > 0$. As a consequence, in the AO phase the Kitaev spin liquid harbors gapless Majorana fermion excitations with linear dispersion about the \mathbf{K} point. This conclusion agrees with the result from the parton mean-field approach in Sec. IV A. Remarkably, the Kitaev spin liquid remains gapless despite the spontaneous breakdown of time-reversal symmetry. In contrast to the effect of a magnetic field in the original Kitaev model [6], here the AO order parameter preserves the symmetry combining time reversal with a C_2 rotation that exchanges A and B sublattices. This symmetry rules out the three-spin interaction that would

drive a nonzero spin chirality in the Kitaev spin liquid and generate a mass term for the Majorana fermions [6].

In the FQV phase, the effective Kitaev couplings \mathcal{K}_{jl}^γ become bond dependent. While the FQV order breaks the \mathbb{Z}_3 symmetry, it preserves a \mathbb{Z}_6 symmetry corresponding to a rotation in real and internal space around the center of the hexagon that defines the enlarged unit cell in Fig. 5. This symmetry implies that there are only two types of Kitaev couplings: $\mathcal{K}_{jl}^\gamma = \mathcal{K}_{\text{in}}$ for bonds inside the unit cell, represented by solid lines in Fig. 5, and $\mathcal{K}_{jl}^\gamma = \mathcal{K}_{\text{out}}$ for bonds connecting neighboring unit cells, represented by dashed lines. Using the linear orbital wave theory, we find $\mathcal{K}_{\text{in}} > 0$ and $\mathcal{K}_{\text{out}} > 0$ with $\mathcal{K}_{\text{out}} \ll \mathcal{K}_{\text{in}}$ regardless of the ratio between K_o and K_q . In this regime, the Majorana spectrum is gapped with weakly dispersive bands. This gapped FQV phase is consistent with the result from the parton mean-field approach. We note that the effect of FQV order on the Majorana fermions in the hidden Kitaev spin liquid is analogous to a Kekulé distortion in graphene, which also triples the size of the unit cell and opens a gap in the spectrum [65, 66].

V. CONCLUSIONS

In summary, we investigated the properties of a model for $j_{\text{eff}} = \frac{3}{2}$ local moments on a honeycomb lattice with bond-directional quadrupolar and octupolar interactions. For special values of the parameters, we obtained an exact solution by representing the $j_{\text{eff}} = \frac{3}{2}$ multipolar operators in terms of two sets of Majorana fermions. This representation allowed us to map the model onto noninteracting fermions hopping in the background of a static \mathbb{Z}_2 gauge field. This model provides a prime example of an interacting system with a nondegenerate ground state, gapless fermionic excitations, and QSL correlations due to the fractionalization of higher-order multipoles.

We demonstrated the emergence of nontrivial topological phases by explicitly breaking rotational and time-reversal symmetries in the MSL. Applying both strain and magnetic fields, we found Abelian and non-Abelian phases with Chern numbers of 0, ± 1 , and ± 2 . The Abelian topological phase with $\mathcal{N}_{\text{Ch}} = \pm 2$ appears for arbitrarily weak perturbations. While Abelian and non-Abelian phases were reported in recent studies of the antiferromagnetic Kitaev model in a magnetic field [67, 68], our model highlights the role of strain as an additional control parameter for driving topological phase transitions between chiral spin-orbital liquid phases.

The stability of the MSL was probed by considering integrability-breaking quadrupolar and octupolar interactions. In the weak-coupling regime, the application of parton mean-field theory showed that the MSL remains stable over a wide range of interaction strengths. This stability can be understood from a renormalization-group point of view by noting that in the fermionic representation the interactions are clearly irrelevant due to

the vanishing density of states of the Dirac nodes in the MSL. When a phase transition out of the MSL finally takes place, the system develops either ferroquadrupolar-vortex or antiferro-octupolar order. The parton mean-field theory leads to a coexistence region at intermediate couplings, but the orbital wave theory at strong coupling indicates a direct first-order transition between the two ordered phases. Despite the spontaneous symmetry breaking, the low-energy spectrum in the strong-coupling regime can be interpreted in terms of a hidden Kitaev spin liquid with effective couplings between pseudospin degrees of freedom. Of course, an important open question is whether the regime of dominant quadrupolar and octupolar interactions considered in this work can be reached in layered materials with $4d$ and $5d$ transition-metal ions [16].

ACKNOWLEDGMENTS

We would like to thank C. S. de Farias, E. Miranda, and W. Natori for interesting discussions with. H.F. acknowledges funding from the Brazilian agency CNPq under Grant No. 311428/2021-5. R.G.P. acknowledges funding from CNPq under Grant No. 309569/2022-2. This work was supported by a grant from the Simons Foundation (Grant No. 1023171, R.G.P.). Research at IIP-UFRN is supported by the Brazilian ministries Ministério da Educação (MEC) and Ministério da Ciência, Tecnologia e Inovação (MCTI).

APPENDIX A: COMPARISON BETWEEN THE ENERGIES OF THE ZERO- AND π -GAUGE FLUX GROUND STATES

In the main text, we stated that the ground state (GS) of the MSL lies in the zero-gauge flux sector $W_p = +1$, which is obtained by setting $u_{(jl)\gamma} = 1$ for sites j in sublattice A and l in sublattice B. To confirm that result, we will compare the GS energy of the MSL for both $W_p = +1$ and $W_p = -1$, in which the latter defines the so-called π -gauge flux sector for this model.

As exemplified in Fig. 9(a), a translationally invariant honeycomb lattice with $W_p = -1$ is obtained with a unit cell containing four sublattice sites. Since the gauge variables for this unit cell evaluate to

$$u_{(3,2)_x} = +1, \quad u_{(3,2)_y} = +1, \quad u_{(1,2)_z} = +1, \quad (\text{A1})$$

$$u_{(1,4)_x} = +1, \quad u_{(1,4)_y} = -1, \quad u_{(3,4)_z} = +1, \quad (\text{A2})$$

we find that the MSL Hamiltonian in Eq. (14) turns out to be

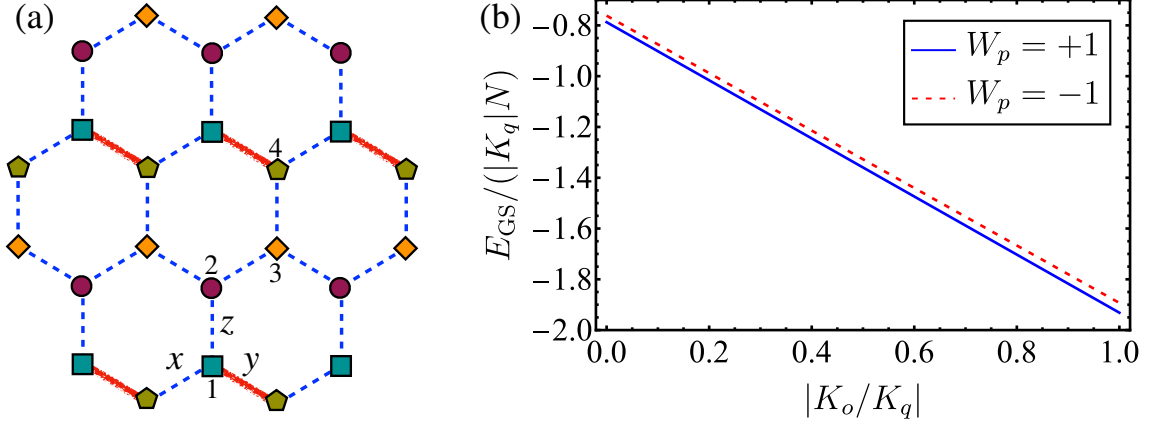


FIG. 9. (a) Honeycomb lattice for a translationally invariant π -gauge flux configuration $W_p = -1$. The dashed blue and filled red bonds refer to the bond variables $u_{\langle jl \rangle \gamma} = +1$ and $u_{\langle jl \rangle \gamma} = -1$, respectively. In terms of this configuration, the physical unit cell contains four sublattices, which are indicated by numbers and also by different regular polygons. (b) Behavior of the MSL GS energies $E_{\text{GS}}^+ \equiv E_{\text{GS}}(\{W_p = +1\})$ and $E_{\text{GS}}^- \equiv E_{\text{GS}}(\{W_p = -1\})$ for the zero- and π -gauge flux configurations, respectively. Note that E_{GS}^+ is always lower than E_{GS}^- , which is consistent with Lieb's theorem [69].

$$H_s = \sum_{\mathbf{k} \in \overline{\text{BZ}}} \bar{\Theta}^\dagger(\mathbf{k}) \begin{pmatrix} 0 & i\Gamma^z(\mathbf{k}) & 0 & i[\Gamma^x(\mathbf{k}) - \Gamma^y(\mathbf{k})] \\ -i\Gamma^{z\dagger}(\mathbf{k}) & 0 & -i[\Gamma^{x\dagger}(\mathbf{k}) + \Gamma^{y\dagger}(\mathbf{k})] & 0 \\ 0 & i[\Gamma^x(\mathbf{k}) + \Gamma^y(\mathbf{k})] & 0 & i\Gamma^z(\mathbf{k}) \\ -i[\Gamma^{x\dagger}(\mathbf{k}) - \Gamma^{y\dagger}(\mathbf{k})] & 0 & -i\Gamma^{z\dagger}(\mathbf{k}) & 0 \end{pmatrix} \bar{\Theta}(\mathbf{k}), \quad (\text{A3})$$

where $\bar{\Theta}(\mathbf{k}) \equiv (\theta_1(\mathbf{k}), \theta_2(\mathbf{k}), \theta_3(\mathbf{k}), \theta_4(\mathbf{k}))^T$; $\overline{\text{BZ}}$ refers to the Brillouin zone associated with the four-sublattice unit cell; and the functions $\Gamma^\gamma(\mathbf{k})$, with $\gamma \in \{x, y, z\}$, represent the following momentum-dependent matrices:

$$\Gamma^x(\mathbf{k}) = \left[K_q \begin{pmatrix} 0 & 0 & 0 \\ 0 & 1 & 0 \\ 0 & 0 & 0 \end{pmatrix} + \frac{K_o}{4} \begin{pmatrix} 1 & 0 & \sqrt{3} \\ 0 & 0 & 0 \\ \sqrt{3} & 0 & 3 \end{pmatrix} \right] e^{-i\mathbf{k} \cdot \boldsymbol{\delta}_1}, \quad (\text{A4})$$

$$\Gamma^y(\mathbf{k}) = \left[K_q \begin{pmatrix} 0 & 0 & 0 \\ 0 & 1 & 0 \\ 0 & 0 & 0 \end{pmatrix} + \frac{K_o}{4} \begin{pmatrix} 1 & 0 & -\sqrt{3} \\ 0 & 0 & 0 \\ -\sqrt{3} & 0 & 3 \end{pmatrix} \right] e^{-i\mathbf{k} \cdot \boldsymbol{\delta}_2}, \quad (\text{A5})$$

$$\Gamma^z(\mathbf{k}) = \left[K_q \begin{pmatrix} 0 & 0 & 0 \\ 0 & 1 & 0 \\ 0 & 0 & 0 \end{pmatrix} + K_o \begin{pmatrix} 1 & 0 & 0 \\ 0 & 0 & 0 \\ 0 & 0 & 0 \end{pmatrix} \right] e^{-i\mathbf{k} \cdot \boldsymbol{\delta}_3}. \quad (\text{A6})$$

Here, $\boldsymbol{\delta}_1$, $\boldsymbol{\delta}_2$, and $\boldsymbol{\delta}_3$ are nearest-neighbor vectors pointing from an even- to an odd-sublattice site in the direction of the x , y , and z bonds, respectively.

The diagonalization of H_s in Eq. (A3) yields $3\bar{N}_s = 12$ energy dispersions $\bar{E}_{s,n}(\mathbf{k})$, but only four of them can be computed in closed form. Since the latter also have a complicated dependence, they will not be displayed here. Regardless, the GS energy $E_{\text{GS}}^- \equiv E_{\text{GS}}(\{W_p = -1\})$ associated with this Hamiltonian can be computed numerically. In fact, its formula is given by

$$\frac{E_{\text{GS}}^-}{N} = \frac{1}{\bar{N}_s} \sum_{n=1}^{3\bar{N}_s} \int_{\overline{\text{BZ}}} \frac{d^2\mathbf{k}}{\mathcal{A}_{\overline{\text{BZ}}}} \bar{E}_n(\mathbf{k}) \Theta[-\bar{E}_{s,n}(\mathbf{k})], \quad (\text{A7})$$

where N refers to the number of sites of the honeycomb lattice, $\mathcal{A}_{\overline{\text{BZ}}} = 4\pi^2/(3\sqrt{3}a^2)$ is the area of the $\overline{\text{BZ}}$, and $\Theta(x)$ denotes the Heaviside step function. This formula should be contrasted with the equation

$$\frac{E_{\text{GS}}^+}{N} = \frac{1}{\bar{N}_s} \sum_{n=1}^{3\bar{N}_s} \int_{\text{BZ}} \frac{d^2\mathbf{k}}{\mathcal{A}_{\text{BZ}}} E_n(\mathbf{k}) \Theta[-E_{s,n}(\mathbf{k})], \quad (\text{A8})$$

which yields the GS energy $E_{\text{GS}}^+ \equiv E_{\text{GS}}(\{W_p = +1\})$ of the MSL in the zero-gauge flux configuration. In this case, the unit cell has $N_s = 2$ sublattices, and $\mathcal{A}_{\text{BZ}} = 8\pi^2/(3\sqrt{3}a^2)$ gives the area of the corresponding BZ. In addition, $E_{s,n}(\mathbf{k})$ refers to $3N_s = 6$ energy dispersions whose expressions can be found in the main text [see Eq.

(16) and the paragraph above it].

In Fig. 9(b), we show the behavior of both E_{GS}^- and E_{GS}^+ as a function of the ratio $|K_o/K_q|$. Clearly, the zero-gauge flux configuration $W_p = +1$ has the lowest GS energy. Moreover, we also investigate the behavior of the GS energy gap per lattice site $(E_{\text{GS}}^- - E_{\text{GS}}^+)/N$. In fact, our numerical results reveal that $(E_{\text{GS}}^- - E_{\text{GS}}^+)/N$ depends linearly on $|K_o/K_q|$. Consequently, we obtain

$$\frac{E_{\text{GS}}^- - E_{\text{GS}}^+}{N} = b_0(|K_o| + 2|K_q|), \quad (\text{A9})$$

where $b_0 \approx 0.012867$. Remarkably, this means that the quadrupolar and octupolar degrees of freedom of the MSL contribute differently to $E_{\text{GS}}^- - E_{\text{GS}}^+$. In other words, the impact of the former is twice that of the latter.

Note that, according to Lieb's theorem [69], the zero-gauge flux configuration yields the lowest-energy GS for

mirror-symmetric models with nearest-neighbor interactions defined on a honeycomb lattice. In light of this result, consider the MSL Hamiltonian H_s in Eq. (14). The first term in H_s involving the θ^y fermions is clearly invariant under a reflection exchanging the x and y bonds since θ^y transforms as the matter Majorana fermions in the Kitaev model for isotropic exchange interactions. However, the mirror symmetry of the term that involves θ^x and θ^z requires the additional transformation $\theta^z \rightarrow -\theta^z$, which can be traced back to the symmetry properties of the quadrupole components (τ^x, τ^z) . We can view $\theta^z \rightarrow -\theta^z$ as a gauge transformation which does not affect the gauge-invariant fluxes nor the spectrum of H_s . For this reason, we expected the result of Lieb's theorem to apply also to our model, which was confirmed by our numerical results.

APPENDIX B: MEAN-FIELD HAMILTONIAN FOR MAJORANA FERMIONS IN THE ZERO-GAUGE FLUX SECTOR

After we fix the uniform gauge configuration for $u_{\langle jl \rangle}$, which is equivalent to setting $W_p = +1$ for all plaquettes, the exactly solvable Hamiltonian can be written as

$$H_s + \delta H_s = \sum_{\mathbf{k}} \Theta^\dagger(\mathbf{k}) \mathcal{H}_s(\mathbf{k}) \Theta(\mathbf{k}), \quad (\text{B1})$$

where $\Theta(\mathbf{k}) \equiv (\theta_A^x(\mathbf{k}), \theta_B^x(\mathbf{k}), \theta_A^y(\mathbf{k}), \theta_B^y(\mathbf{k}), \theta_A^z(\mathbf{k}), \theta_B^z(\mathbf{k}))^T$ and we define the matrix

$$\mathcal{H}_s(\mathbf{k}) = \begin{pmatrix} 0 & iK_o g_x(\mathbf{k}) & i\varepsilon_3 & 0 & -ih & iK_o g_{xz}(\mathbf{k}) \\ -K_o g_x^*(\mathbf{k}) & 0 & 0 & i\varepsilon_3 & -iK_o g_{xz}^*(\mathbf{k}) & -ih \\ -i\varepsilon_3 & 0 & 0 & iK_q g_y(\mathbf{k}) & i\varepsilon_2 & 0 \\ 0 & -i\varepsilon_3 & -iK_q g_y^*(\mathbf{k}) & 0 & 0 & i\varepsilon_2 \\ ih & iK_o g_{xz}(\mathbf{k}) & -i\varepsilon_2 & 0 & 0 & iK_o g_z(\mathbf{k}) \\ -iK_o g_{xz}^*(\mathbf{k}) & ih & 0 & -i\varepsilon_2 & -iK_o g_z(\mathbf{k}) & 0 \end{pmatrix}, \quad (\text{B2})$$

with the functions given below Eq. (16). Here we have included the perturbations that determine the phase diagram in Fig. 3. In the parton mean-field theory in Sec. IV A, we set $\varepsilon_2 = \varepsilon_3 = h = 0$.

According to Eqs. (22) and (23), the mean-field decoupling of the Hamiltonian $H = H_s + H_I$ leads to

$$H_{\text{MF}} = \sum_{\mathbf{k} \in \frac{1}{6}(\text{BZ})} \begin{pmatrix} \Theta(\mathbf{k}) \\ \Theta(\mathbf{k} + \mathbf{Q}_1) \\ \Theta(\mathbf{k} + \mathbf{Q}_2) \end{pmatrix}^\dagger \begin{pmatrix} \mathcal{H}_s(\mathbf{k}) + \mathcal{V} & \mathcal{V}_{\mathbf{Q}_1} & \mathcal{V}_{\mathbf{Q}_2} \\ \mathcal{V}_{\mathbf{Q}_1}^\dagger & \mathcal{H}_s(\mathbf{k} + \mathbf{Q}_1) + \mathcal{V} & 0 \\ \mathcal{V}_{\mathbf{Q}_2}^\dagger & 0 & \mathcal{H}_s(\mathbf{k} + \mathbf{Q}_2) + \mathcal{V} \end{pmatrix} \begin{pmatrix} \Theta(\mathbf{k}) \\ \Theta(\mathbf{k} + \mathbf{Q}_1) \\ \Theta(\mathbf{k} + \mathbf{Q}_2) \end{pmatrix} \\ - \frac{K'_q}{2} N \rho^2 \sum_{\mu=1}^2 \sum_{\gamma=1}^3 [f_\mu^\gamma(\varphi)]^2 \cos(\mathbf{Q}_\mu \cdot \boldsymbol{\delta}_\gamma) + \frac{3K'_o}{2} N \chi^2, \quad (\text{B3})$$

where we have set

$$\mathcal{V}_{\mathbf{Q}_\mu} = 3K'_q \begin{pmatrix} 0 & 0 & i\rho_{\mu,A}^{xy*} & 0 & 0 & 0 \\ 0 & 0 & 0 & i\rho_{\mu,B}^{xy} & 0 & 0 \\ -i\rho_{\mu,A}^{xy*} & 0 & 0 & 0 & -i\rho_{\mu,A}^{yz*} & 0 \\ 0 & -i\rho_{\mu,B}^{xy} & 0 & 0 & 0 & -i\rho_{\mu,B}^{yz} \\ 0 & 0 & i\rho_{\mu,A}^{yz*} & 0 & 0 & 0 \\ 0 & 0 & 0 & i\rho_{\mu,B}^{yz} & 0 & 0 \end{pmatrix}, \quad (\text{B4})$$

$$\mathcal{V} = 6K'_o \begin{pmatrix} 0 & 0 & 0 & 0 & -i\chi & 0 \\ 0 & 0 & 0 & 0 & 0 & i\chi \\ 0 & 0 & 0 & 0 & 0 & 0 \\ 0 & 0 & 0 & 0 & 0 & 0 \\ i\chi & 0 & 0 & 0 & 0 & 0 \\ 0 & -i\chi & 0 & 0 & 0 & 0 \end{pmatrix}. \quad (\text{B5})$$

The matrices $\mathcal{V}_{\mathbf{Q}_\mu}$ are defined in terms of the functions

$$\rho_{\mu,A}^{xy} = \frac{\rho}{2} \left[\frac{f_\mu^1(\varphi)e^{i\mathbf{Q}_\mu \cdot \delta_1} + f_\mu^2(\varphi)e^{i\mathbf{Q}_\mu \cdot \delta_2}}{2} - f_\mu^3(\varphi)e^{i\mathbf{Q}_\mu \cdot \delta_3} \right], \quad (\text{B6})$$

$$\rho_{\mu,A}^{yz} = \frac{\sqrt{3}\rho}{4} [-f_\mu^1(\varphi)e^{i\mathbf{Q}_\mu \cdot \delta_1} + f_\mu^2(\varphi)e^{i\mathbf{Q}_\mu \cdot \delta_2}], \quad (\text{B7})$$

$$\rho_{\mu,B}^{xy} = \frac{\rho}{2} \left[\frac{f_\mu^1(\varphi)e^{i\mathbf{Q}_\mu \cdot \mathbf{n}_1} + f_\mu^2(\varphi)e^{i\mathbf{Q}_\mu \cdot \mathbf{n}_2}}{2} - f_\mu^3(\varphi) \right], \quad (\text{B8})$$

$$\rho_{\mu,B}^{yz} = \frac{\sqrt{3}\rho}{4} [-f_\mu^1(\varphi)e^{i\mathbf{Q}_\mu \cdot \mathbf{n}_1} + f_\mu^2(\varphi)e^{i\mathbf{Q}_\mu \cdot \mathbf{n}_2}]. \quad (\text{B9})$$

-
- [1] L. Balents, Spin liquids in frustrated magnets, *Nature* **464**, 199 (2010).
- [2] C. Broholm, R. J. Cava, S. A. Kivelson, D. G. Nocera, M. R. Norman, and T. Senthil, Quantum spin liquids, *Science* **367**, eaay0668 (2020).
- [3] L. Savary and L. Balents, Quantum spin liquids: a review, *Rep. Prog. Phys.* **80**, 016502 (2017).
- [4] H. Takagi, T. Takayama, G. Jackeli, G. Khaliullin, and S. E. Nagler, Concept and realization of Kitaev quantum spin liquids, *Nat. Rev. Phys.* **1**, 264 (2019).
- [5] S. Trebst and C. Hickey, Kitaev materials, *Phys. Rep.* **950**, 1 (2022).
- [6] A. Kitaev, Anyons in an exactly solved model and beyond, *Ann. Phys.* **321**, 2 (2006).
- [7] G. Jackeli and G. Khaliullin, Mott Insulators in the Strong Spin-Orbit Coupling Limit: From Heisenberg to a Quantum Compass and Kitaev Models, *Phys. Rev. Lett.* **102**, 017205 (2009).
- [8] Y. Singh and P. Gegenwart, Antiferromagnetic Mott insulating state in single crystals of the honeycomb lattice material Na_2IrO_3 , *Phys. Rev. B* **82**, 064412 (2010).
- [9] Y. Singh, S. Manni, J. Reuther, T. Berlijn, R. Thomale, W. Ku, S. Trebst, and P. Gegenwart, Relevance of the Heisenberg-Kitaev Model for the Honeycomb Lattice Iridates $A_2\text{IrO}_3$, *Phys. Rev. Lett.* **108**, 127203 (2012).
- [10] G. Cao, T. F. Qi, L. Li, J. Terzic, V. S. Cao, S. J. Yuan, M. Tovar, G. Murthy, and R. K. Kaul, Evolution of magnetism in the single-crystal honeycomb iridates $(\text{Na}_{1-x}\text{Li}_x)_2\text{IrO}_3$, *Phys. Rev. B* **88**, 220414 (2013).
- [11] K. Kitagawa, T. Takayama, Y. Matsumoto, A. Kato, R. Takano, Y. Kishimoto, S. Bette, R. Dinnebier, G. Jackeli, and H. Takagi, A spin-orbital-entangled quantum liquid on a honeycomb lattice, *Nature (London)* **554**, 341 (2018).
- [12] K. W. Plumb, J. P. Clancy, L. J. Sandilands, V. V. Shankar, Y. F. Hu, K. S. Burch, H.-Y. Kee, and Y.-J. Kim, α - RuCl_3 : A spin-orbit assisted Mott insulator on a honeycomb lattice, *Phys. Rev. B* **90**, 041112 (2014).
- [13] Y. Kasahara, T. Ohnishi, Y. Mizukami, O. Tanaka, S. Ma, K. Sugii, N. Kurita, H. Tanaka, J. Nasu, Y. Motome, T. Shibauchi, and Y. Matsuda, Majorana quantization and half-integer thermal quantum Hall effect in a Kitaev spin liquid, *Nature (London)* **559**, 227 (2018).
- [14] O. Tanaka, Y. Mizukami, R. Harasawa, K. Hashimoto, K. Hwang, N. Kurita, H. Tanaka, S. Fujimoto, Y. Matsuda, E.-G. Moon, and T. Shibauchi, Thermodynamic evidence for a field-angle-dependent Majorana gap in a Kitaev spin liquid, *Nat. Phys.* **1**, 1 (2022).
- [15] W. Witczak-Krempa, G. Chen, Y. B. Kim, and L. Balents, Correlated Quantum Phenomena in the Strong Spin-Orbit Regime, *Annu. Rev. Condens. Matter Phys.* **5**, 57 (2014).
- [16] T. Takayama, J. Chaloupka, A. Smerald, G. Khaliullin, and H. Takagi, Spin-Orbit-Entangled Electronic Phases in 4d and 5d Transition-Metal Compounds, *J. Phys. Soc. Jpn.* **90**, 062001 (2021).
- [17] P. P. Stavropoulos, D. Pereira, and H.-Y. Kee, Microscopic Mechanism for a Higher-Spin Kitaev Model, *Phys.*

- Rev. Lett. **123**, 037203 (2019).
- [18] C. Xu, J. Feng, M. Kawamura, Y. Yamaji, Y. Nahas, S. Prokhorenko, Y. Qi, H. Xiang, and L. Bellaïche, Possible Kitaev Quantum Spin Liquid State in 2D Materials with $S = 3/2$, *Phys. Rev. Lett.* **124**, 087205 (2020).
- [19] C. Xu, J. Feng, H. Xiang, and L. Bellaïche, Interplay between Kitaev interaction and single ion anisotropy in ferromagnetic CrI_3 and CrGeTe_3 monolayers, *npj Comput. Mater.* **4**, 57 (2018).
- [20] P. P. Stavropoulos, X. Liu, and H.-Y. Kee, Magnetic anisotropy in spin-3/2 with heavy ligand in honeycomb Mott insulators: Application to CrI_3 , *Phys. Rev. Res.* **3**, 013216 (2021).
- [21] G. Baskaran, D. Sen, and R. Shankar, Spin- S Kitaev model: Classical ground states, order from disorder, and exact correlation functions, *Phys. Rev. B* **78**, 115116 (2008).
- [22] A. Koga, H. Tomishige, and J. Nasu, Ground-state and Thermodynamic Properties of an $S = 1$ Kitaev Model, *J. Phys. Soc. Jpn.* **87**, 063703 (2018).
- [23] C. Hickey, C. Berke, P. P. Stavropoulos, H.-Y. Kee, and S. Trebst, Field-driven gapless spin liquid in the spin-1 Kitaev honeycomb model, *Phys. Rev. Res.* **2**, 023361 (2020).
- [24] X.-Y. Dong and D. N. Sheng, Spin-1 Kitaev-Heisenberg model on a honeycomb lattice, *Phys. Rev. B* **102**, 121102 (2020).
- [25] Z. Zhu, Z.-Y. Weng, and D. N. Sheng, Magnetic field induced spin liquids in $S = 1$ Kitaev honeycomb model, *Phys. Rev. Res.* **2**, 022047 (2020).
- [26] I. Khait, P. P. Stavropoulos, H.-Y. Kee, and Y. B. Kim, Characterizing spin-one Kitaev quantum spin liquids, *Phys. Rev. Res.* **3**, 013160 (2021).
- [27] H.-K. Jin, W. M. H. Natori, F. Pollmann, and J. Knolle, Unveiling the $S = 3/2$ Kitaev honeycomb spin liquids, *Nat. Commun.* **13**, 3813 (2022).
- [28] G. Chen, R. Pereira, and L. Balents, Exotic phases induced by strong spin-orbit coupling in ordered double perovskites, *Phys. Rev. B* **82**, 174440 (2010).
- [29] W. M. H. Natori, E. C. Andrade, E. Miranda, and R. G. Pereira, Chiral Spin-Orbital Liquids with Nodal Lines, *Phys. Rev. Lett.* **117**, 017204 (2016).
- [30] W. M. H. Natori, M. Daghofer, and R. G. Pereira, Dynamics of a $j = \frac{3}{2}$ quantum spin liquid, *Phys. Rev. B* **96**, 125109 (2017).
- [31] J. Romhányi, L. Balents, and G. Jackeli, Spin-Orbit Dimers and Noncollinear Phases in d^1 Cubic Double Perovskites, *Phys. Rev. Lett.* **118**, 217202 (2017).
- [32] W. M. H. Natori, E. C. Andrade, and R. G. Pereira, $\text{SU}(4)$ -symmetric spin-orbital liquids on the hyperhoneycomb lattice, *Phys. Rev. B* **98**, 195113 (2018).
- [33] M. G. Yamada, M. Oshikawa, and G. Jackeli, Emergent $\text{SU}(4)$ Symmetry in $\alpha\text{-ZrCl}_3$ and Crystalline Spin-Orbital Liquids, *Phys. Rev. Lett.* **121**, 097201 (2018).
- [34] H. Ishikawa, T. Takayama, R. K. Kremer, J. Nuss, R. Dinnebier, K. Kitagawa, K. Ishii, and H. Takagi, Ordering of hidden multipoles in spin-orbit entangled $5d^1$ Ta chlorides, *Phys. Rev. B* **100**, 045142 (2019).
- [35] C. S. de Farias, V. S. de Carvalho, E. Miranda, and R. G. Pereira, Quadrupolar spin liquid, octupolar Kondo coupling, and odd-frequency superconductivity in an exactly solvable model, *Phys. Rev. B* **102**, 075110 (2020).
- [36] G. Chen and C. Wu, Mott insulators with large local Hilbert spaces in quantum materials and ultracold atoms, *arXiv:2112.02630* (2021).
- [37] W. M. H. Natori, H.-K. Jin, and J. Knolle, Quantum liquids of the $S = 3/2$ Kitaev honeycomb and related Kugel-Khomskii models, *arXiv:2304.13378* (2023).
- [38] Y.-D. Li and G. Chen, Symmetry enriched $\text{U}(1)$ topological orders for dipole-octupole doublets on a pyrochlore lattice, *Phys. Rev. B* **95**, 041106 (2017).
- [39] R. Sibille, N. Gauthier, E. Lhotel, V. Porée, V. Pomjakushin, R. A. Ewings, T. G. Perring, J. Ollivier, A. Wildes, C. Ritter, T. C. Hansen, D. A. Keen, G. J. Nilsen, L. Keller, S. Petit, and T. Fennell, A quantum liquid of magnetic octupoles on the pyrochlore lattice, *Nat. Phys.* **16**, 546 (2020).
- [40] A. Rayyan, D. Churchill, and H.-Y. Kee, Field-induced Kitaev multipolar liquid in spin-orbit coupled d^2 honeycomb Mott insulators, *Phys. Rev. B* **107**, L020408 (2023).
- [41] D. I. Khomskii and S. V. Streltsov, Orbital effects in solids: Basics, recent progress, and opportunities, *Chem. Rev.* **121**, 2992 (2021).
- [42] S. V. Streltsov and D. I. Khomskii, Jahn-Teller Effect and Spin-Orbit Coupling: Friends or Foes? *Phys. Rev. X* **10**, 031043 (2020).
- [43] J. G. Rau, E. K.-H. Lee, and H.-Y. Kee, Generic Spin Model for the Honeycomb Iridates beyond the Kitaev Limit, *Phys. Rev. Lett.* **112**, 077204 (2014).
- [44] J. M. Baker, Interactions between ions with orbital angular momentum in insulators, *Rep. Prog. Phys.* **34**, 109 (1971).
- [45] G. A. Gehring and K. A. Gehring, Co-operative Jahn-Teller effects, *Rep. Prog. Phys.* **38**, 1 (1975).
- [46] S. Voleti, A. Haldar, and A. Paramakanti, Octupolar order and Ising quantum criticality tuned by strain and dimensionality: Application to d -orbital Mott insulators, *Phys. Rev. B* **104**, 174431 (2021).
- [47] R. Yadav, S. Rachel, L. Hozoi, J. van den Brink, and G. Jackeli, Strain- and pressure-tuned magnetic interactions in honeycomb Kitaev materials, *Phys. Rev. B* **98**, 121107 (2018).
- [48] P. Santini, S. Carretta, G. Amoretti, R. Caciuffo, N. Magnani, and G. H. Lander, Multipolar interactions in f -electron systems: The paradigm of actinide dioxides, *Rev. Mod. Phys.* **81**, 807 (2009).
- [49] N. Iwahara, V. Vieru, and L. F. Chibotaru, Spin-orbital-lattice entangled states in cubic d^1 double perovskites, *Phys. Rev. B* **98**, 075138 (2018).
- [50] C. Wu, Orbital Ordering and Frustration of p -Band Mott Insulators, *Phys. Rev. Lett.* **100**, 200406 (2008).
- [51] G. Khaliullin, D. Churchill, P. P. Stavropoulos, and H.-Y. Kee, Exchange interactions, Jahn-Teller coupling, and multipole orders in pseudospin one-half $5d^2$ Mott insulators, *Phys. Rev. Research* **3**, 033163 (2021).
- [52] K. Kubo and Y. Kuramoto, Lattice Distortion and Octupole Ordering Model in $\text{Ce}_x\text{La}_{1-x}\text{B}_6$, *J. Phys. Soc. Jpn.* **72**, 1859 (2003).
- [53] K. Kubo and Y. Kuramoto, Octupole Ordering Model for the Phase IV of $\text{Ce}_x\text{La}_{1-x}\text{B}_6$, *J. Phys. Soc. Jpn.* **73**, 216 (2004).
- [54] A. Paramakanti, D. D. Maharaj, and B. D. Gaulin, Octupolar order in d -orbital Mott insulators, *Phys. Rev. B* **101**, 054439 (2020).
- [55] D. Churchill and H.-Y. Kee, Competing multipolar orders in a face-centered cubic lattice: Application to the osmium double perovskites, *Phys. Rev. B* **105**, 014438 (2022).

- [56] R. Shiina, H. Shiba, and P. Thalmeier, Magnetic-Field Effects on Quadrupolar Ordering in a Γ_8 -Quartet System CeB_6 , *J. Phys. Soc. Jpn.* **66**, 1741 (1997).
- [57] J. Knolle, D. L. Kovrizhin, J. T. Chalker, and R. Moessner, Dynamics of a Two-Dimensional Quantum Spin Liquid: Signatures of Emergent Majorana Fermions and Fluxes, *Phys. Rev. Lett.* **112**, 207203 (2014).
- [58] T. Fukui, Y. Hatsugai, and H. Suzuki, Chern Numbers in Discretized Brillouin Zone: Efficient Method of Computing (Spin) Hall Conductances, *J. Phys. Soc. Jpn.* **74**, 1674 (2005).
- [59] S.-S. Zhang, C. D. Batista, and G. B. Halász, Toward Kitaev's sixteenfold way in a honeycomb lattice model, *Phys. Rev. Res.* **2**, 023334 (2020).
- [60] S. Chulliparambil, U. F. P. Seifert, M. Vojta, L. Janssen, and H.-H. Tu, Microscopic models for Kitaev's sixteenfold way of anyon theories, *Phys. Rev. B* **102**, 201111(R) (2020).
- [61] R. M. Fernandes, P. P. Orth, and J. Schmalian, Intertwined Vestigial Order in Quantum Materials: Nematicity and Beyond, *Annu. Rev. Condens. Matter Phys.* **10**, 133 (2019).
- [62] G. Murthy, D. Arovas, and A. Auerbach, Superfluids and supersolids on frustrated two-dimensional lattices, *Phys. Rev. B* **55**, 3104 (1997).
- [63] E. Zhao and W. V. Liu, Orbital Order in Mott Insulators of Spinless p -Band Fermions, *Phys. Rev. Lett.* **100**, 160403 (2008).
- [64] J. van den Brink, W. Stekelenburg, D. I. Khomskii, G. A. Sawatzky, and K. I. Kugel, Elementary excitations in the coupled spin-orbital model, *Phys. Rev. B* **58**, 10276 (1998).
- [65] C.-Y. Hou, C. Chamon, and C. Mudry, Electron Fractionalization in Two-Dimensional Graphenelike Structures, *Phys. Rev. Lett.* **98**, 186809 (2007).
- [66] A. C. Qu and P. Nigge and S. Link and G. Levy and M. Michiardi and P. L. Spandar and T. Matthé and M. Schneider and S. Zhdanovich and U. Starke and C. Gutiérrez and A. Damascelli, Ubiquitous defect-induced density wave instability in monolayer graphene, *Sci. Adv.* **8**, eabm5180 (2022).
- [67] M.-H. Jiang, S. Liang, W. Chen, Y. Qi, J.-X. Li, and Q.-H. Wang, Tuning Topological Orders by a Conical Magnetic Field in the Kitaev Model, *Phys. Rev. Lett.* **125**, 177203 (2020).
- [68] S.-S. Zhang, G. B. Halász, and C. D. Batista, Theory of the Kitaev model in a [111] magnetic field, *Nat. Commun.* **13**, 399 (2022).
- [69] E. H. Lieb, Flux Phase of the Half-Filled Band, *Phys. Rev. Lett.* **73**, 2158 (1994).